





## Experimental and density functional theory study on structure, vibrational and molecular characteristics of 2-chloro-5-methylpyrimidine and 2,4-dichloro-5-methylpyrimidine

B. Sreenivas, L. Ravindranath, K. Srishailam, Jai Kishan Ojha & B. Venkatram Reddy

To cite this article: B. Sreenivas, L. Ravindranath, K. Srishailam, Jai Kishan Ojha & B. Venkatram Reddy (2022): Experimental and density functional theory study on structure, vibrational and molecular characteristics of 2-chloro-5-methylpyrimidine and 2,4-dichloro-5-methylpyrimidine, Molecular Simulation, DOI: [10.1080/08927022.2022.2060967](https://doi.org/10.1080/08927022.2022.2060967)

To link to this article: <https://doi.org/10.1080/08927022.2022.2060967>

 View supplementary material 

 Published online: 08 Apr 2022.

 Submit your article to this journal 

 View related articles 

 View Crossmark data 



# Experimental and density functional theory study on structure, vibrational and molecular characteristics of 2-chloro-5-methylpyrimidine and 2,4-dichloro-5-methylpyrimidine

B. Sreenivas<sup>a</sup>, L. Ravindranath<sup>a</sup>, K. Srishailam<sup>a,b</sup>, Jai Kishan Ojha<sup>c</sup> and B. Venkatram Reddy <sup>a</sup>

<sup>a</sup>Department of Physics, Kakatiya University, Warangal, India; <sup>b</sup>Department of Physics, SR University, Warangal, India; <sup>c</sup>Department of Physics, Government Degree College, Mancherla, India

## ABSTRACT

This study deals with the determination of torsional potentials, optimised geometry in monomer and dimer form for gas phase for the molecular ground state and vibrational assignments of 2-chloro-5-methyl pyrimidine; and 2,4-dichloro-5-methyl pyrimidine carried out by density functional theory employing B3LYP exchange and correlational functional in conjunction with 6-311++G(d,p) basis set using quantum chemical calculations. The existence of inter-molecular hydrogen bonds was also predicted. Fourier Transform infrared and Fourier Transform Raman spectra were recorded and vibrational analysis of the molecules was made using potential energy distribution and eigen vectors obtained in the computations. Observed and calculated frequencies agreed with an rms error 10.03 and 10.0 cm<sup>-1</sup> for 2-chloro-5-methyl pyrimidine and 2,4-dichloro-5-methyl pyrimidine, respectively. Electronic transitions were analysed using experimental and simulated Ultraviolet-Visible spectra of the two molecules wherein polarisable, continuum model in solvent phase was used for simulations. Molecular characteristics like highest occupied molecular orbital, lowest unoccupied molecular orbital, molecular electrostatic surface potential and thermodynamic parameters were also investigated. Stability of the molecules arising from hyper conjugative interactions, charge delocalisation has been analysed using natural bond orbital analysis.

## ARTICLE HISTORY

Received 30 September 2021  
Accepted 28 March 2022

## KEYWORDS

Chloro-methylpyrimidine;  
DFT; HOMO-LUMO; NBO;  
MESP

## 1. Introduction

In our earlier articles, we used a method for theoretical determination of dihedral angles around flexible bonds for biphenylcarboxaldehydes [1] and extended it to dimethylbipyridines [2], and dihydroxytoluenes [3]. The method involves exhaustive torsional potential energy scans about bonds that exhibit internal rotation, leading to the evaluation of their structural parameters based on the theoretical approach alone. To test this method further for its efficacy, we have chosen 2-chloro-5-methylpyrimidine (CM) and 2,4-dichloro-5-methylpyrimidine (DCM) in this investigation and reported results obtained therefrom.

Pyrimidine is a model compound for biologically significant heterocyclic molecules that consist of four carbons and two nitrogen atoms at positions 1 and 3 in the aromatic ring. It plays a key role in several natural and non-natural products [4]. Pyrimidine derivatives are known for their potential utility in a very wide range of applications in coordination chemistry, pharmaceuticals, medicine, biochemistry and agrochemicals. They occupy a prominent role as anti-inflammatory [5–9], antitumour [10], analgesic [11], anticancer [12–14] and HIV-1 reverse transcriptase inhibiting drugs [15]. Krajlevic et al. [16] reported the synthesis, X-ray crystal structure and antitumoral evaluations of 5,6-disubstituted pyrimidine derivatives. These derivatives were investigated for their cytostatic activities against human malignant cell lines and they

were also studied for hydrogen bonds. Szterner et al. [17] reported the standard molar enthalpies of formation in the condensed phase evaluated from the standard molar energies of combustion and the gas-phase enthalpies of formation obtained by G3 theoretical computations of some dichloromethylpyrimidines. Joshi [18] reported the analysis of structural, electronic and vibrational study of 4,6-dichloro-5-methylpyrimidine using density functional theory (DFT) computations. Medjani et al. [19] reported the crystal structure of 4,6-dichloro-5-methylpyrimidine using X-ray diffraction (XRD) studies. Furberg et al. [20] studied the change in the structure of pyrimidine with the substitution of chlorine, methyl and amino moieties and compared the differences in electron density maps among them.

Hence, the literature review reveals that the two compounds 2-chloro-5-methylpyrimidine (CM) and 2,4-dichloro-5-methylpyrimidine (DCM) were not investigated for their molecular and vibrational characteristics except the determination of molar enthalpies of vapourisation and gas-phase enthalpies of formation for thermochemical analysis by Szterner et al. [17]. Hence, it is thought to enhance available knowledge on the two molecules by investigating the following aspects.

- (1) Recording Fourier transform infrared (FT-IR) and Fourier transform Raman (FT Raman) spectra of CM and DCM, and

- (2) Performing density functional theory(DFT) computations for the molecules in order to:
- make torsional potential energy scans for different angles of rotation around inter-linking C–C bond between the pyrimidine ring and methyl group to get the approximate values of associated dihedral angles for each of the two molecules,
  - perform geometry optimisation in the gas phase by using dihedral angles in conjunction with bond lengths and bond angles were taken from the Gauss view [21] for monomers of the two molecules,
  - use monomer structure for optimising the geometry of dimers of both molecules in the gas phase,
  - study intra- and inter-molecular hydrogen bonds
  - calculate harmonic vibrational frequencies and assign them to ensure the quality of obtained force constants to meet the mandatory requirement,
  - record Ultraviolet–Visible spectra arising from electronic transitions,
  - evaluate the molecular properties such as highest occupied molecular orbital(HOMO) and lowest unoccupied molecular orbital (LUMO)energies, molecular electrostatic surface potential (MESP), thermodynamic parameters and rotational constants, and
  - study the stability of the molecules in terms of hyper conjugative interactions and charge delocalisation obtained from natural bond orbital (NBO) analysis.

## 2. Materials and experimental methods

High-purity solid samples 2-chloro-5-methylpyrimidine and 2,4-dichloro-5-methylpyrimidine were procured from TCI chemical company and recorded their spectra without further purification. The FT-IR spectra of these samples were recorded in the spectral range 4000–4450  $\text{cm}^{-1}$  by diluting them in KBr pellet, using Nicolet-740 single beam FT-IR spectrometer, equipped with deuterated triglycine sulphate (DTGS) detector. The FT Raman spectra of the samples were measured, in the 4000–4050  $\text{cm}^{-1}$  Stokes region, using BRUKER RFS-27 accessory employing the exciting radiation at 1064 nm provided by Nd-YAG laser operating at 200 mw power. UV-Vis absorption spectral data of the samples in a solution of DMSO-d<sub>6</sub> using 1 cm quartz cell was obtained in the range of 200–400 nm on Perkin-Elmer UV-Visible LAMBDA-25 double beam spectrophotometer.

## 3. Computational details

The quantum chemical computations in respect of molecular geometry optimization, vibrational analysis, frontier molecular orbital analysis and natural bond orbital analysis of CM and DCM were carried out by applying the density functional theory (DFT) method as implemented in Gaussian 09 program [22]. Becke's non-local gradient approach to the exchange functional in its three-parameter hybrid density form (B3) [23] along with Lee, Young and Parr gradient corrected correlation functional (LYP) [24] in conjunction with triple zeta split-valence basis set, 6-311++G(d,p) was employed for the

computations. The geometries were fully optimised with the default convergence principle without any limitation by using a systematic procedure employed with Gaussian 09 program [22] for isolated molecules CM and DCM. This implies that the calculations were performed in the gas phase. Relative infrared absorption intensities were calculated following the method proposed by Latajka et al. [25]. Similarly, relative Raman scattering intensities were computed according to the procedure put forward by Kerezthury et al. [26,27]. For the plots of simulated FT-IR and Raman spectra, pure Lorentzian band shape with full width at half maximum (FWHM) of 10  $\text{cm}^{-1}$  was employed. Multiple scaling of force field has been carried out by Scaled Quantum Mechanical (SQM) procedure [28–30] in the natural internal coordinate representation [31] to offset the systematic errors caused by the basis set incompleteness, incomplete implementation of electron correlation and neglect of vibrational anharmonicity effects to obtain good frequency fit between observed and calculated values. The force constants obtained in the process were transformed into a non-redundant set of natural internal coordinates obtained from redundant internal coordinates following the procedure suggested by Fogarasi et al. [31]. Normal coordinate analysis, calculation of potential energy distribution (PED) and prediction of infrared and Raman intensities were made using MOLVIB 7.0 program written by Sundius [32,33]. The simulated Gaussian output was visualised using the Gauss View 5.0 program [21]. The electronic transitions were computed with Time-Dependent Density Functional Theory (TD-DFT), employing the same functional and basis set used in the DFT computations. Natural bond orbital (NBO) analysis was performed using NBO 3.1 program [34] as implemented in the Gaussian 09 package with the 6-311++G(d,p) basis set in order to understand various second-order interactions between the filled orbitals of one subsystem and vacant orbitals of another subsystem following second-order perturbation theory as used by Fock matrix method.

## 4. Results and discussion

### 4.1. Molecular geometry in the ground state

Geometry optimisation is the most fundamental requirement, which is an integral part of electronic structure methods aimed at understanding vibrational properties and molecular characteristics. To initiate geometry optimisation for a given molecule in DFT computations, a preliminary structure is essential in the process. If the information on basic structure is not available experimentally, it is usual practice that the initial structure for a given molecule can be generated by using the experimental structure parameters of a related molecule and by taking help from Gauss View [21]. The bond lengths and bond angles obtained in this way have adequate accuracy. But, the corresponding dihedral angles of a rotating bond of a molecule are known to change over a wide range of values in large molecules [35]. It implies that the starting parameters are incompatible in terms of their accuracy. This incomparability is likely to reveal itself by generating negative or imaginary frequencies in the process of geometry optimisation. The solution for such a problem can be obtained by

Gaussian 09 program suit [22] using DFT formalism as shown in our earlier articles [1–3]. The method involves torsional potential energy scans at different fixed values of dihedral angle with spacing  $5^\circ$  or  $10^\circ$  between two consecutive values about a given rotating bond by fixing all other structure parameters and spanning the entire conformational space from  $0^\circ$  to  $360^\circ$ .

Now, both the molecules have only one bond about which rotation is permitted. This is the C–C inter-link bond between the pyrimidine ring and methyl group (C5–C10 bond in Figures 2 and 3). Hence, the torsional potential energy was computed as a function of the angle of rotation around this bond in steps of  $5^\circ$  between  $0^\circ$  and  $360^\circ$  to determine the preliminary values of dihedral angles using the Gaussian 09W software package implemented on Pentium-V (3.2 GHz) workstation. These computations yielded a six-fold potential energy curve with minimum energy at  $0^\circ$  for CM and a three-fold potential energy curve with minimum energy at  $180^\circ$  for DCM. Using the above data, potential energy scan plots were drawn between the relative energy and dihedral angle around the inter-link C–C bond for both the molecules and are depicted in Figure 1.

Values of dihedral angles so obtained for CM and DCM were used in conjunction with other structural parameters transferred from the related molecule 4,6-dichloro-5-methylpyrimidine [19], drawing considerable help from the Gauss view [21] to generate the required starting structure. This was subjected to geometry optimisation by relaxing all structural parameters by solving self-consistent field equations iteratively. This process yielded a  $C_1$  stable monomeric structure with minimum energy  $-2004.167 \times 10^3 \text{ kJ mol}^{-1}$  ( $-479.007 \times 10^3 \text{ kcal mol}^{-1}$ ) and  $-3210.912 \times 10^3 \text{ kJ mol}^{-1}$  ( $-767.426 \times 10^3 \text{ kcal mol}^{-1}$ ) for CM and DCM, respectively and are shown in Figures 2 and 3. The absence of imaginary

or negative frequencies in the computations substantiates the fact that the structures correspond to the ground state. The  $C_1$  symmetry was used as equilibrium reference geometry for the subsequent computations for the evaluation of Cartesian force constants, vibrational frequencies and the values of other molecular parameters for the two molecules.

Optimised geometry for the dimers of CM and DCM, obtained from the corresponding monomer structure, is shown in Figures 4 and 5, along with the numbering of atoms, hydrogen bond lengths and minimum energy. The optimised structure parameters consisting of bond lengths, bond angles and dihedral angles, for both monomers and dimers of CM and DCM, and the parameters corresponding to the inter-molecular hydrogen bond of dimers are presented in Table 1. The theoretically calculated parameters are also compared in Table 1 with the experimental values obtained from the XRD analysis of the related molecule [19].

#### 4.1.1. Monomer

Both molecules, CM and DCM, stabilise in the ground state in non-planar configuration of  $C_1$  symmetry. This is due to balance between two opposing effects: conjugation of  $\pi$ -electrons of the pyrimidine ring and lone pair of nitrogen and chlorine atoms favouring planar configuration and steric repulsion between the bulky methyl moiety and its ortho neighbours favouring non-planar structure. From Table 1 it is evident that the calculated structure parameters of CM and DCM are in reasonable agreement with those obtained experimentally from XRD studies for related molecules 2-chloropyrimidine [20] and 4,6-dichloro-5-methylpyrimidine [19]. For example, the average value of C–N and C–C bond length computed as 1.329 and 1.396 Å for CM monomer is in good

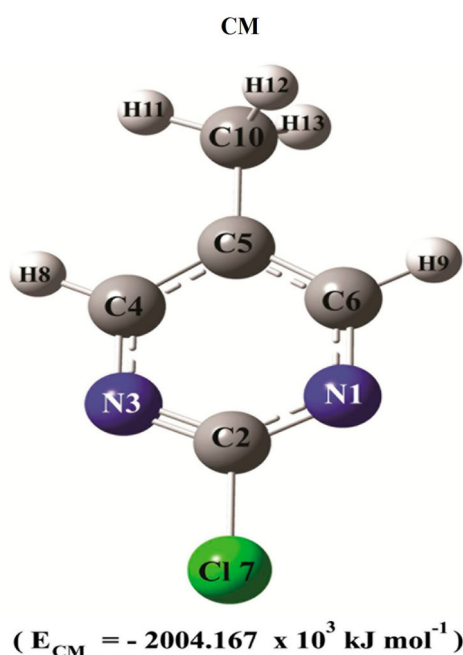


**Figure 2.** (Colour online) Optimised molecular structure of CM monomer along with numbering of atoms.

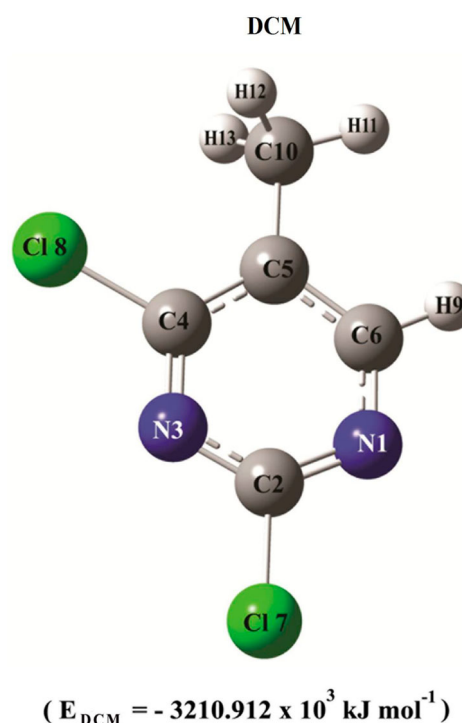


**Figure 3.** (Colour online) Optimised molecular structure of DCM monomer along with numbering of atoms.

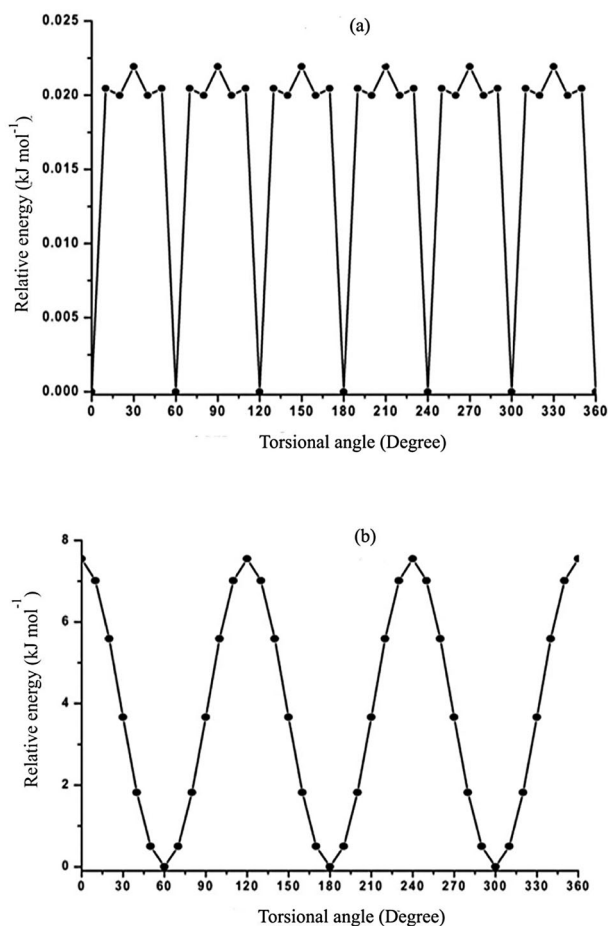


**Figure 1.** Relative torsional potential energy as a function of rotation angle (C4-C5-C10-H11) for (a) CM and (b) DCM using DFT/B3LYP/6-311++G(d, p) formalism.

agreement with their experimental value 1.335 and 1.388 Å, respectively obtained for 2-chloropyrimidine [20]. Similarly, for the DCM monomer, the average value of computed bond lengths 1.325 and 1.398 Å of C-N and C-C bonds agree well

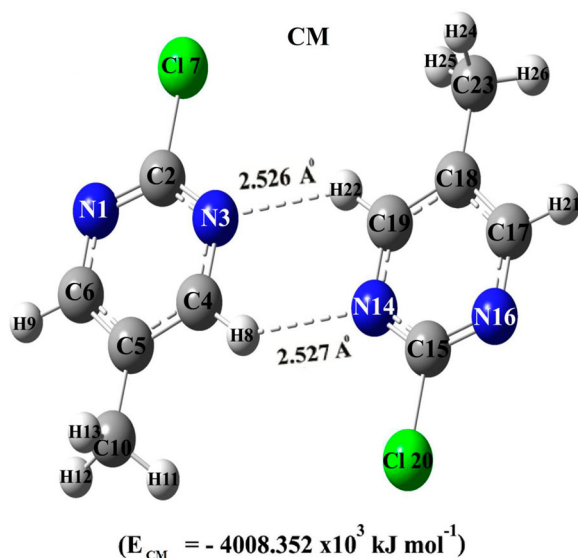


**Figure 4.** (Colour online) Optimised molecular structure of CM dimer along with numbering of atoms, inter-molecular hydrogen bonding and minimum energy.

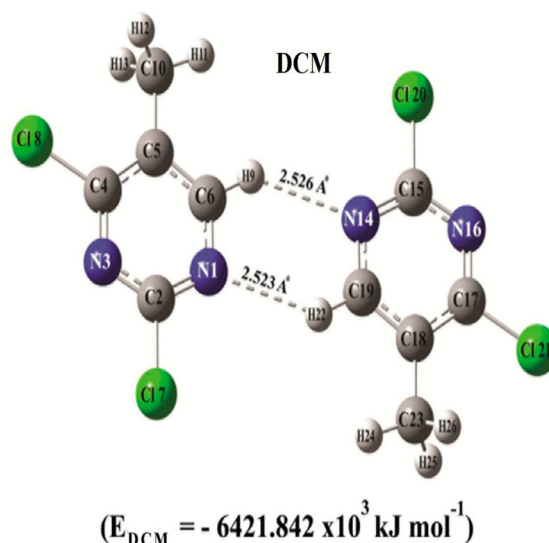


**Figure 5.** (Colour online) Optimised molecular structure of DCM dimer along with numbering of atoms, inter-molecular hydrogen bonding and minimum energy.

with X-ray diffraction values 1.319 and 1.399 Å, respectively, obtained for 4,6-dichloro-5-methylpyrimidine [19]. Similarly, the length of C-Cl bond computed at 1.752 Å for CM monomer; and 1.747 and 1.752 Å for DCM is also agree well, respectively, with the observed value 1.735 Å of 2-chloropyrimidine [20]; and 1.737 and 1.737 Å of 4,6-dichloro-5-methylpyrimidine [19].

#### 4.1.2. Dimer and inter-molecular hydrogen bonding

A dimer can be considered as a supra molecule formed by hydrogen bonding between two stable monomers of lowest energy conformation. In the test molecules, two nitrogen atoms of the pyrimidine ring of one monomer participate in hydrogen bonding with the nearest hydrogen atoms of the pyrimidine ring of other monomer, giving rise to dimers. The resultant structure was subjected to geometry optimisation with simultaneous relaxation of all structural parameters, as in the case of monomer. This process yielded  $C_1$  symmetry for the dimeric structures of both CM and DCM. The optimised geometry obtained for dimers of CM and DCM, along with numbering of atoms is depicted in Figures 4 and 5, respectively. Their structure parameters are collected in Table 1, along with their corresponding monomers. As the optimised geometry of both monomer and dimer of the two molecules was obtained using the same level of theory, their relative values are reliable.

The minimum energy for the dimeric structure of CM and DCM is  $-4008.352 \times 10^3 \text{ kJ mol}^{-1}$  ( $-958.019 \times 10^3 \text{ kcal mol}^{-1}$ ) and  $-6421.842 \times 10^3 \text{ kJ mol}^{-1}$  ( $-1534.857 \times 10^3 \text{ kcal mol}^{-1}$ ), respectively. It is an established fact that if the minimum energy of a dimer is less than twice the minimum energy of its monomer, then the formation of dimer is favoured. It can be seen that, for both CM and DCM, the minimum energy of dimers is less by  $0.018 \times 10^3 \text{ kJ mol}^{-1}$  and hence, the formation of dimers of CM and DCM.

From Figures 4 and 5, and Table 1, it can be seen that the calculated hydrogen bond lengths are: N3...H22 = 2.526 Å

**Table 1.** Experimental and theoretical geometrical parameters with the DFT/B3LYP/6-311++G(d,p) optimised geometric parameters of CM, DCM and their dimers.

Geometric parameter	CM		DCM		Expt. value	
	Calculated value		Calculated value		Furberg <sup>a</sup>	Medjani <sup>b</sup>
	Monomer	Dimer	Monomer	Dimer		
<b>Bond lengths ( in Å )</b>						
N1-C2	1.325	1.322	1.320	1.320	1.326	1.327
C2-N3	1.322	1.323	1.326	1.324	1.329	1.335
N3-C4	1.336	1.339	1.318	1.319	1.343	1.315
C4-C5	1.395	1.396	1.402	1.401	1.386	1.403
C5-C6	1.397	1.396	1.395	1.395	1.390	1.395
C6-N1	1.334	1.336	1.336	1.341	1.344	1.299
C2-Cl7	1.752	1.757	1.747	1.750	1.735	1.737
C4-H8	1.087	1.087	–	–	0.950	0.930
C4-Cl8	–	–	1.752	1.751	–	1.737
C6-H9	1.088	1.087	1.087	1.087	0.950	0.930
C5-C10	1.504	1.505	1.500	1.500	–	1.486
C10-H11	1.091	1.092	1.091	1.091	–	0.960
C10-H12	1.093	1.094	1.093	1.093	–	0.960
C10-H13	1.093	1.092	1.093	1.093	–	0.960
<b>Bond angle ( in ° )</b>						
N1-C2-N3	127.70	127.85	127.24	127.37	129.0	126.8
C2-N3-C4	115.56	115.77	115.94	115.81	114.6	114.8
N3-C4-C5	123.29	122.74	124.08	124.11	122.7	125.7
C4-C5-C6	114.61	114.93	113.29	113.56	116.5	111.4
C5-C6-N1	123.26	123.27	124.15	123.67	122.3	125.9
C6-N1-C2	115.57	115.43	115.29	115.48	114.9	115.4
Cl7-C2-N1	116.09	116.14	116.73	116.56	115.8	*
Cl7-C2-N3	116.21	116.00	116.03	116.07	115.2	*
H8-C4-N3	115.91	115.56	–	–	115.0	*
H8-C4-C5	120.79	121.70	–	–	121.0	*
Cl8-C4-N3	–	–	116.18	116.10	–	115.1
Cl8-C4-C5	–	–	119.74	119.79	–	119.2
H9-C6-C5	120.89	120.89	119.87	120.79	120.0	*
H9-C6-N1	115.84	115.83	115.97	115.54	116.0	*
C10-C5-C4	122.82	122.40	124.24	124.23	–	125.2
C10-C5-C6	122.56	122.66	122.46	122.20	–	123.4
C5-C10-H11	110.99	111.14	110.50	110.44	–	109.5
C5-C10-H12	111.22	110.95	111.18	111.15	–	109.5
C5-C10-H13	111.22	111.30	111.18	111.15	–	109.5
H11-C10-H12	107.87	107.48	108.38	108.44	–	109.5
H12-C10-H13	107.50	107.55	107.08	107.09	–	109.5
H13-C10-H11	107.87	108.24	108.38	108.44	–	109.5
<b>Dihedral angle ( in ° )</b>						
N1-C2-N3-C4	0.00	–0.52	0.00	0.00	*	–0.7
C2-N3-C4-C5	0.00	0.14	0.00	0.00	*	1.3
N3-C4-C5-C6	0.00	–0.66	0.00	0.00	*	–1.1
C4-C5-C6-N1	0.00	0.66	0.00	0.00	*	0.1
C5-C6-N1-C2	0.00	0.10	0.00	0.00	*	0.5
C6-N1-C2-N3	0.00	0.54	0.00	0.00	*	0.2
C6-N1-C2-Cl7	180.00	179.69	180.00	179.99	*	*
C4-N3-C2-Cl7	180.00	179.70	180.00	179.99	*	*
C2-N3-C4-H8	180.00	179.62	–	–	*	*
C6-C5-C4-H8	180.00	179.08	–	–	*	*
C2-N3-C4-Cl8	–	–	180.00	179.99	–	178.9
C6-C5-C4-Cl8	–	–	180.00	179.99	–	179.2
C4-C5-C6-H9	180.00	179.12	180.00	179.99	*	*
C2-N1-C6-H9	180.00	179.67	180.00	179.99	*	*
N3-C4-C5-C10	180.00	178.73	180.00	180.00	–	179.5
N1-C6-C5-C10	180.00	178.75	180.00	180.00	–	179.5
C4-C5-C10-H11	0.00	26.80	180.00	179.99	–	*
C4-C5-C10-H12	120.10	92.74	59.60	59.60	–	*
C4-C5-C10-H13	–120.10	–147.53	59.60	59.60	–	*
<b>Inter-molecular H-bond length and bond angle of Dimers</b>						
Geometric parameter	Bond length ( in Å )			Bond Angle ( in ° )		
	CM	DCM	Exp <sup>b</sup>	CM	DCM	Exp <sup>b</sup>
C2-N3.....H22	2.527	–	2.660	140.94	–	146.00
C15-N14.....H8	2.527	–	2.660	140.95	–	146.00
C2-N1.....H22	–	2.523	2.660	–	139.82	146.00
C15-N14.....H9	–	2.526	2.660	–	139.88	146.00
C4.....N14	3.442	–	3.468	–	–	–
C19.....N3	3.442	–	3.468	–	–	–
C6.....N14	–	3.428	3.468	–	–	–
C19.....N1	–	3.426	3.468	–	–	–

Note: Å, angstrom; °, degree; –, Not relevant; \*, not available.

<sup>a</sup>From reference 19.

<sup>b</sup>From reference 18.

and N14.....H8 = 2.527 Å for CM; and N1.....H22 = 2.523 Å and N14.....H9 = 2.526 Å for DCM. Steiner reported in a review article that though the hydrogen bonds formed in a range of lengths due to different interactions, the electrostatic component is the dominant in the medium and long-range hydrogen bonds [36]. It was also suggested that the hydrogen bonds having bond distances in the range 2.4–2.8 Å may be considered as weak. The lengths estimated for C2-N3.....H22 and C15-N14.....H8 in CM; and those for C2-N1.....H22 and C15-N14.....H9 in DCM dimers fall in the range 2.4–2.8 Å. Hence, they may be considered as weak. The length of bonds of both C4.....N14 and C19.....N3 is evaluated as 3.442 Å in CM; and that of C6.....N14 and C19.....N1 bonds is estimated at 3.428 and 3.426 Å, respectively, in DCM. These bond lengths are >2.8 Å, and hence they are likely to be due to weak Van der Waals interactions. Steiner and Desiraju [37,38] stated that it is impossible to define an exact border cone between the hydrogen bonding region and Van der Waals interaction space in a molecule. However, hydrogen bond interactions may be evaluated easily by using Bader's theory of 'Atoms in Molecules' implemented in AIM2000 software updated by Biegler-könig and Schönbohm [39] in 2002.

## 4.2. Vibrational analysis

In order to gain better insight into vibrational modes of CM and DCM, DFT studies were carried out at B3LYP/6-311G (d,p) level of theory for the gas phase. The number of atoms in each of the molecules CM and DCM is 13. Hence, each molecule has 33 vibrational frequencies according to the formula  $3n-6$ , where 'n' is the number of atoms in the molecule. All of them belong to a-species in  $C_1$  symmetry, and are active in both infrared and Raman processes.

Observed (both FT-IR and FT Raman) and computed (scaled) frequencies of CM and DCM are summarised in Table 2, while the computed IR and Raman intensities and potential energy distribution (PED) of these molecules are presented as supplementary information in Tables S1 and S2. Vibrations originating from the pyrimidine nucleus were designated by Wilson's notation [40]. The experimental and simulated FT-IR and FT-Raman spectra are compared in Figures 6 and 7; and Figures 8 and 9, respectively, for CM and DCM.

The calculated frequencies are in good agreement with experimental values with an estimated rms error of 10.03 and 10.0  $\text{cm}^{-1}$  for CM and DCM, respectively. This can be understood from Table 2 and supplementary Tables S1 and S2. Hence, the structure for both molecules CM and DCM may be considered as correct. The vibrational assignments presented in the Table 2 and supplementary Tables S1 and S2 are self-explanatory and hence, the discussion is restricted to some important bands observed in FT-IR and FT Raman spectra for CM and DCM.

### 4.2.1. Vibrations of 2-chloro-5-methylpyrimidine (CM)

A pair of strong bands observed at 1389 and 1574  $\text{cm}^{-1}$  in FT-IR, and 1391 and 1577  $\text{cm}^{-1}$  in FT Raman spectra are assigned to C–N stretching vibration, which are in good agreement with DFT scaled values at 1417 and 1592  $\text{cm}^{-1}$ , respectively in CM.

A strong Raman absorption at 3048  $\text{cm}^{-1}$  with corresponding simulated value at 3057  $\text{cm}^{-1}$  is assigned to mode 7a, which represents C–H stretching vibration. Similarly, a pair of strong peaks observed in Raman at 406 and 644  $\text{cm}^{-1}$ , which match with computed values near 407 and 638  $\text{cm}^{-1}$  are attributed to ring torsion (mode 16a) and ring vibration (mode 6b), respectively. Strong bands observed in FT-IR spectrum at 605, 762 and 1149  $\text{cm}^{-1}$  and their corresponding calculated frequencies at 615, 763 and 1146  $\text{cm}^{-1}$  are ascribed to ring vibration (mode 6a), ring torsion (mode 4) and C–C (inter-link bond between pyrimidine ring and methyl group) stretching vibration (mode 13), respectively. Two very strong absorptions in Raman at 838 and 2924  $\text{cm}^{-1}$  corresponding to simulated frequencies of 830 and 2921  $\text{cm}^{-1}$  are attributed to C–N stretching vibration (mode 1) and asymmetric out-of-phase stretching vibration of methyl moiety, respectively, in CM.

### 4.2.2. Vibrations of 2,4-dichloro-5-methylpyrimidine (DCM)

Experimentally observed strong bands at 860 (853R) (R indicates Raman shift), 1562 (1564R), 3055R, 1099, 407R, 1045, 665R, 2928 (2929R), and 1374  $\text{cm}^{-1}$  which are in proximity with simulated frequencies at 845, 1548, 3055, 1102, 412, 1063, 657, 2928 and 1374  $\text{cm}^{-1}$  are assigned based on the PED obtained in the computations to the vibrations C–N stretching (mode 1), C–C stretching (mode 8b), C–H stretching (mode 2), C–C stretching vibration (inter-link bond between pyrimidine ring and methyl group) (mode 13), in-plane bending (inter-link bond) (mode 15), ring vibration (mode 12), ring vibration (mode 6b), out of plane asymmetric stretching of methyl moiety and symmetric bending of methyl group, respectively, in DCM.

It can be observed from the supplementary information given in Table S1 and S2 that the vibrations of the methyl group, substituted at the fifth position of the pyrimidine ring, of the titled molecules are independent as they do not mix among themselves and originating with any other mode of vibration. Hence, the assignment of the vibrational modes originating from the methyl group is not difficult. The vibrational assignments made for methyl group of the molecules under investigation agree nicely with those made for methyl group in related molecules reported in our earlier papers [2,41,42].

## 4.3. Ultraviolet–Visible spectral and Frontier molecular orbitals analyses

UV-Visible absorption spectra are in routine use for quantitative estimation of organic molecules in a solution. However, the presence of impurities is a common problem in organic synthesis, for which the solution phase is preferred. For quantitative analysis of such a solution one has to separate the different components or re-synthesis the impurities alone separately. Such a procedure is both expensive and time-consuming, hence, several alternative methods have been developed, to address this problem, which aim to simulate UV-Visible spectra using theoretical methods. In a recent article Parrish et al. [43] extended variational quantum eigensolver formalism for

**Table 2.** Summary of vibrational assignments, observed and scaled calculated frequencies (in  $\text{cm}^{-1}$ ) of CM and DCM.

Mode <sup>a</sup>	CM			Mode <sup>a</sup>	DCM		
	Obs. freq		Scaled cal. Freq.		Obs. freq		Scaled cal. Freq.
	IR	Raman			IR	Raman	
<i>(i) Vibrations of Pyrimidine</i>							
$\pi(\text{C}(\text{C}1)17\text{b})$	–	70	99	$\pi(\text{C}(\text{C}1)17\text{b})$	–	71	94
$\beta(\text{C}(\text{C}1)9\text{a})$	–	229	230	$\pi(\text{C}(\text{C}1)17\text{a})$	–	–	161
$\pi(\text{C}-\text{CH}_3)11$	–	260	265	$\beta(\text{C}(\text{C}1)9\text{b})$	–	178	177
$\beta(\text{C}-\text{CH}_3)15$	–	333	341	$\beta(\text{C}(\text{C}1)9\text{a})$	–	231	228
$\nu(\text{C}-\text{Cl})7\text{b}$	–	383	383	$\pi(\text{C}-\text{CH}_3)11$	–	277	271
$\tau(\text{C}(\text{C}(\text{C}(\text{C}1)16\text{a}))$	–	406	407	$\nu(\text{C}-\text{Cl})7\text{b}$	–	331	322
$\tau(\text{C}(\text{C}(\text{C}(\text{C}1)16\text{b}))$	455	–	461	$\nu(\text{C}-\text{Cl})7\text{a}$	–	–	347
$\beta(\text{C}(\text{C}(\text{C}1)6\text{a}))$	605	–	615	$\beta(\text{C}-\text{CH}_3)15$	–	407	412
$\beta(\text{C}(\text{C}(\text{C}1)6\text{b}))$	640	644	638	$\tau(\text{C}(\text{C}(\text{C}(\text{C}1)16\text{a}))$	–	434	438
$\tau(\text{C}(\text{C}(\text{C}(\text{C}1)4))$	762	763	763	$\tau(\text{C}(\text{C}(\text{C}(\text{C}1)16\text{b}))$	557	–	560
$\nu(\text{C}-\text{N})1$	836	838	830	$\beta(\text{C}(\text{C}(\text{C}1)6\text{a}))$	–	616	609
$\pi(\text{C}(\text{H})17\text{a})$	915	–	915	$\beta(\text{C}(\text{C}(\text{C}1)6\text{b}))$	664	665	657
$\pi(\text{C}(\text{H})5)$	979	–	980	$\tau(\text{C}(\text{C}(\text{C}(\text{C}1)4))$	759	765	755
$\beta(\text{C}(\text{C}(\text{C}1)12)$	1012	–	1027	$\nu(\text{C}-\text{N})1$	860	853	845
$\nu(\text{C}-\text{CH}_3)13$	1149	1151	1146	$\pi(\text{C}(\text{H})5)$	937	–	937
$\beta(\text{C}(\text{H})9\text{b})$	1237	1242	1212	$\beta(\text{C}(\text{C}(\text{C}1)12)$	1045	–	1063
$\nu(\text{C}-\text{N})14$	–	–	1228	$\nu(\text{C}-\text{CH}_3)13$	1099	–	1102
$\beta(\text{C}(\text{H})3)$	–	–	1262	$\nu(\text{C}-\text{N})14$	1248	1244	1212
$\nu(\text{C}-\text{C})19\text{b}$	–	–	1370	$\beta(\text{C}(\text{H})3)$	–	–	1248
$\nu(\text{C}-\text{N})19\text{a}$	1389	1391	1417	$\nu(\text{C}-\text{C})19\text{b}$	1319	1312	1318
$\nu(\text{C}-\text{C})8\text{b}$	1552	1553	1552	$\nu(\text{C}-\text{N})19\text{a}$	1392	–	1390
$\nu(\text{C}-\text{N})8\text{a}$	1574	1577	1592	$\nu(\text{C}-\text{C})8\text{b}$	1562	1564	1548
$\nu(\text{C}(\text{H})7\text{a})$	3044	3048	3057	$\nu(\text{C}-\text{N})8\text{a}$	–	1604	1604
$\nu(\text{C}-\text{H})2$	3072	–	3072	$\nu(\text{C}-\text{H})2$	–	3055	3055
<i>(ii) Vibrations of Methyl group</i>							
$\tau(\text{C}(\text{H}_3))$	–	–	20	$\tau(\text{C}(\text{H}_3))$	–	109	139
$\gamma(\text{C}(\text{H}_3)_{\text{ip}})$	–	–	1006	$\gamma(\text{C}(\text{H}_3)_{\text{ip}})$	1004	–	1003
$\gamma(\text{C}(\text{H}_3)_{\text{op}})$	1052	1045	1051	$\gamma(\text{C}(\text{H}_3)_{\text{op}})$	–	–	1059
$\delta_s(\text{C}(\text{H}_3))$	–	1376	1376	$\delta_s(\text{C}(\text{H}_3))$	1374	1371	1374
$\delta_{\text{as}}(\text{C}(\text{H}_3)_{\text{op}})$	1450	1455	1450	$\delta_{\text{as}}(\text{C}(\text{H}_3)_{\text{op}})$	1446	1439	1446
$\delta_{\text{as}}(\text{C}(\text{H}_3)_{\text{ip}})$	1476	–	1478	$\delta_{\text{as}}(\text{C}(\text{H}_3)_{\text{ip}})$	–	1473	1473
$\nu_s(\text{C}(\text{H}_3))$	–	2874	2874	$\nu_s(\text{C}(\text{H}_3))$	–	2860	2860
$\nu_{\text{as}}(\text{C}(\text{H}_3)_{\text{op}})$	2921	2924	2921	$\nu_{\text{as}}(\text{C}(\text{H}_3)_{\text{op}})$	2928	2929	2928
$\nu_{\text{as}}(\text{C}(\text{H}_3)_{\text{ip}})$	–	2976	2976	$\nu_{\text{as}}(\text{C}(\text{H}_3)_{\text{ip}})$	2960	2962	2960

Note: –, Not observed.

<sup>a</sup>Mode in Wilson's notation [40].  $\nu$ , stretching;  $\beta$ , in-plane bending;  $\delta$ , deformation;  $\gamma$ , rocking;  $\pi$ , out-of-plane bending;  $\tau$ , torsion; s, symmetric; as, asymmetric; ip, in-phase; op, out-of-phase.

computing electronic transitions and listed a number of theoretical methods that are useful for this purpose, including density functional theory. Our preference, for time-dependent density functional theory (TD-DFT), has two reasons: it has been established by several researchers [44–46] that TD-DFT provides reasonably good results regarding UV-Visible spectral parameters and its usage is in conformity with the general purpose of this article.

Quantum chemical methods generate UV-Visible spectrum in the form of a ray or line spectrum. But, the experimental counterpart has a modified or broad shape. This is due to line-broadening effects (e.g. natural line width, Doppler Effect, thermal excitement). Hence, there is a need to widen each theoretical line or ray spectrum with a Gaussian shape [47,48]. To this end, an integrated approach has been proposed to simulate UV-Visible absorption spectra [49]. The transitions obtained by TD-DFT are the starting point in this procedure. Then, they are modified for each Gaussian function by independent optimisation of full width at half maximum (FWHM). This approach has been found to improve the agreement between observed and computed spectra [49]. From the above, it should be evident that one should not expect perfect

or near-perfect agreement between experimental and theoretical values: one of the plausible reasons for this is that it is not possible to mimic line-broadening effects perfectly, at the present stage of our knowledge.

We used a well-known three-step process [50,51] to simulate the UV-Visible spectra of CM and DCM. These are:

- (1) Full optimisation of the ground state geometry until the mandatory requirement is achieved, i.e. the root-mean-square of forces is less than  $3.0 \times 10^{-4}$  a.u
- (2) Analytical determination of vibrational frequencies to ascertain that the structures correspond to true minima, i.e. absence of imaginary or negative frequencies, and
- (3) Computation of vertical transitions to the valence excited states. The first two steps are implemented in the DFT model, whereas the last one is performed with its time-dependent counterpart, i.e. TD-DFT

Time-dependent density functional theory (TD-DFT) was employed using B3LYP/6-311++G(d,p) formalism in order to simulate electronic absorption spectra of CM and DCM in a solution of DMSO-*d*6 (this is the solvent used to measure



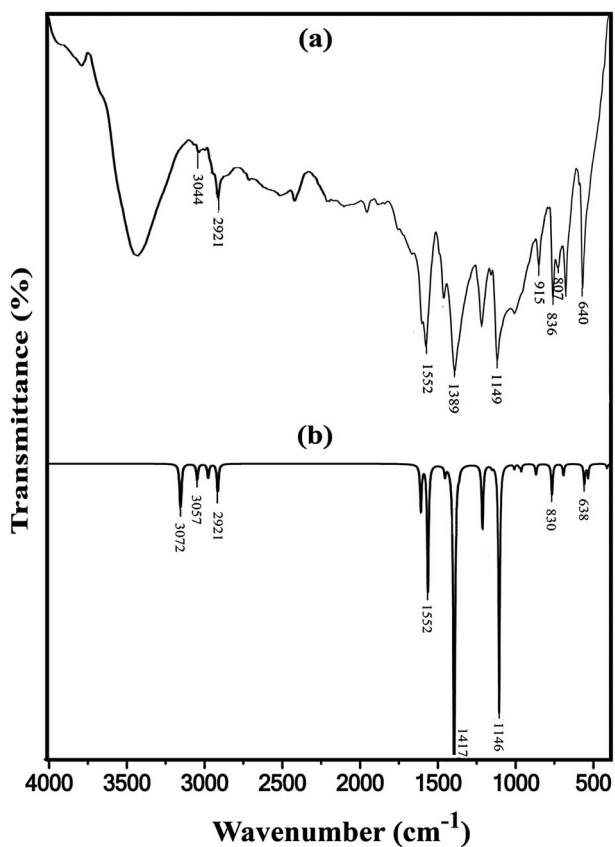


**Figure 6.** FT-IR Spectrum of CM (a) Experimental and (b) Simulated with DFT/B3LYP/6-311++G(d,p) formalism.

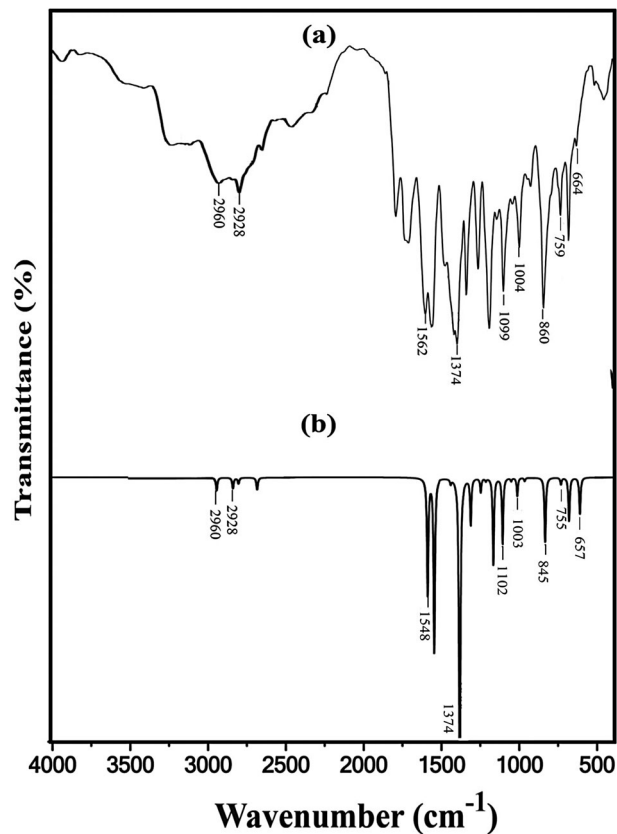


**Figure 8.** FT-IR Spectrum of DCM (a) Experimental and (b) Simulated with DFT/B3LYP/6-311++G(d,p) formalism.

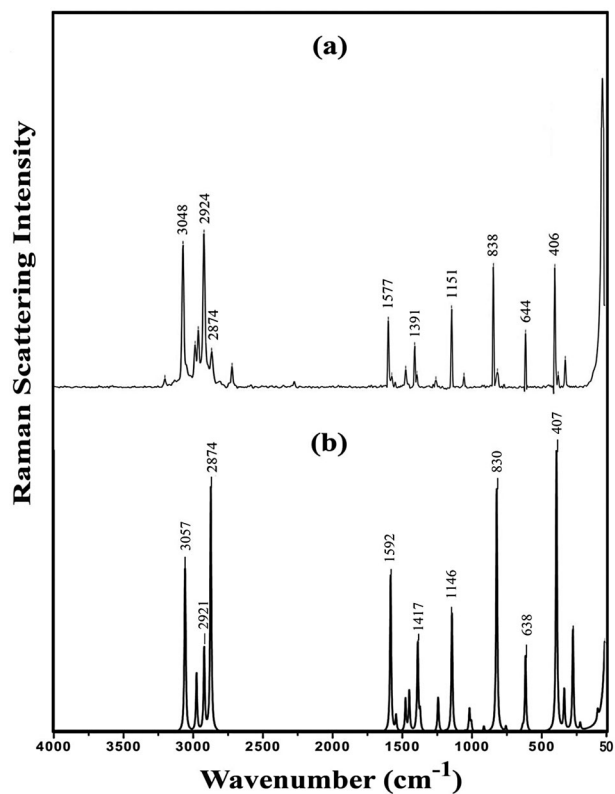


**Figure 7.** FT Raman Spectrum of CM (a) Experimental and (b) Simulated with DFT/B3LYP/6-311++G(d,p) formalism.

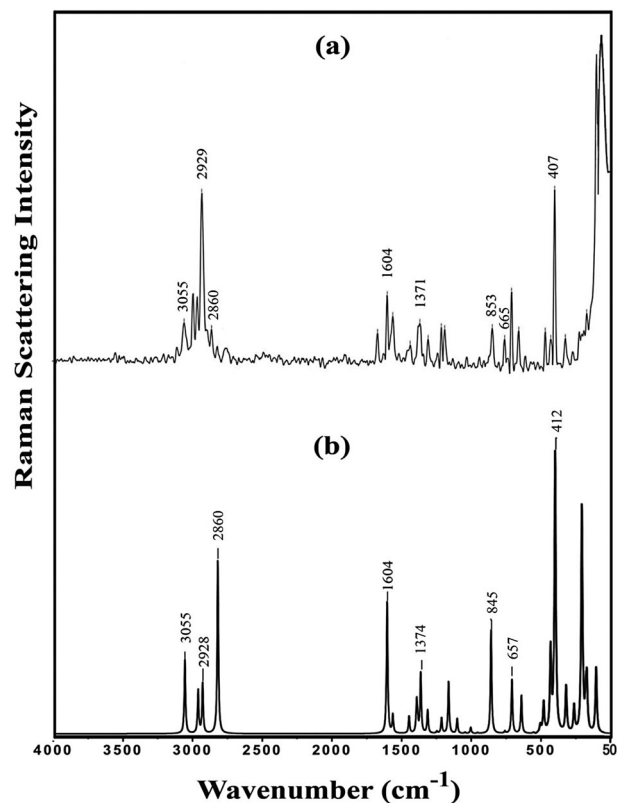


**Figure 9.** FT Raman Spectrum of DCM (a) Experimental and (b) Simulated with DFT/B3LYP/6-311++G(d,p) formalism.

observed spectra). To account for solvent effects, we used the Polarizable Continuum Model (PCM) through the integrated equation formalism (IEF-PCM) variant [52] integrated into Gaussian 09 program package. The experimental and computed spectra for CM and DCM are compared in Figure 10. Computed absorption maxima and related parameters are listed in Table 3.

According to the computations, CM should have two electronic transitions with maxima at  $\lambda_{\max} = 278.59$  and  $242.24$  nm with corresponding oscillator strengths  $f = 0.0061$  and  $0.0607$ , respectively. These are in fair agreement with the corresponding observed electronic transitions near  $\lambda_{\max} = 259.9$  and  $212.1$  nm, which is evident, from Table 3 for CM. Similarly, for DCM, the theory predicts two absorption maxima around  $\lambda_{\max} = 265.81$  and  $245.73$  nm with associated oscillator strengths  $f = 0.0055$  and  $0.0989$ , respectively. These are also agreeing fairly with their experimental counterparts near  $\lambda_{\max} = 263.9$  and  $217.5$  nm for DCM.

Frontier molecular orbitals are very helpful in understanding the electronic transitions presented in the preceding paragraph. We know that the highest occupied molecular orbital (HOMO) and the lowest unoccupied molecular (LUMO) are known together as frontier molecular orbitals. They show the capability of a molecule to absorb electromagnetic radiation. HOMO acts as the electron donor, whereas LUMO plays the role of an electron acceptor [53,54]. Based on the TD-DFT computations, it can be inferred that the experimental bands stated in the preceding paragraph arise mainly due to  $H \rightarrow L$  and  $H-1 \rightarrow L$  transitions, respectively ( $H$  and  $L$  denote HOMO and LUMO, respectively).  $H \rightarrow L$  and  $H-1 \rightarrow L$

**Table 3.** Experimental and theoretical electronic absorption spectral values of CM and DCM.

	Absorption Maximum $\lambda_{\max}(\text{nm})$		Excitation energies (eV)	Oscillator strengths (f)	Transition
	Experimental	Calculated			
CM	259.9	278.59	4.386	0.0061	$n \rightarrow \pi^*$
	212.1	242.24	5.092	0.0607	$\pi \rightarrow \pi^*$
	–	249.79	4.963	0.0000	For bidden
DCM	263.9	265.81	4.610	0.0055	$n \rightarrow \pi^*$
	217.5	245.73	5.031	0.0989	$\pi \rightarrow \pi^*$
	–	243.89	5.0836	0.0001	For bidden
	–	–	–	–	–

transitions can be attributed to  $n \rightarrow \pi^*$  and  $\pi \rightarrow \pi^*$  transitions in CM and DCM, respectively. These are shown in Figure 11.

Frontier molecular orbitals determine the molecular reactivity of conjugated systems [55]. Related parameters calculated employing DFT/B3LYP/6-311++G(d,p) procedure are collected in Table 4, for CM and DCM. The difference between the HOMO and LUMO orbital energies is known as energy gap. This quantity is calculated at  $3.2248$  and  $3.6232$  eV for CM and DCM, respectively, using the data in Table 4. These are low values comparatively, characteristic of conjugated systems. This indicates high chemical reactivity of CM and DCM, as accumulation of electrons in high-lying LUMO by exciting electrons from low-lying HOMO is energetically favourable. Further, a molecule with a small frontier orbital gap exhibits three characteristics, (i) it is easily polarisable, (ii) it is usually highly reactive chemically and (iii) it has low kinetic stability [56–58]. It is to be noted that, as the chemical potential ( $\mu$ ) is negative (see Table 4), both the molecules are stable [59].

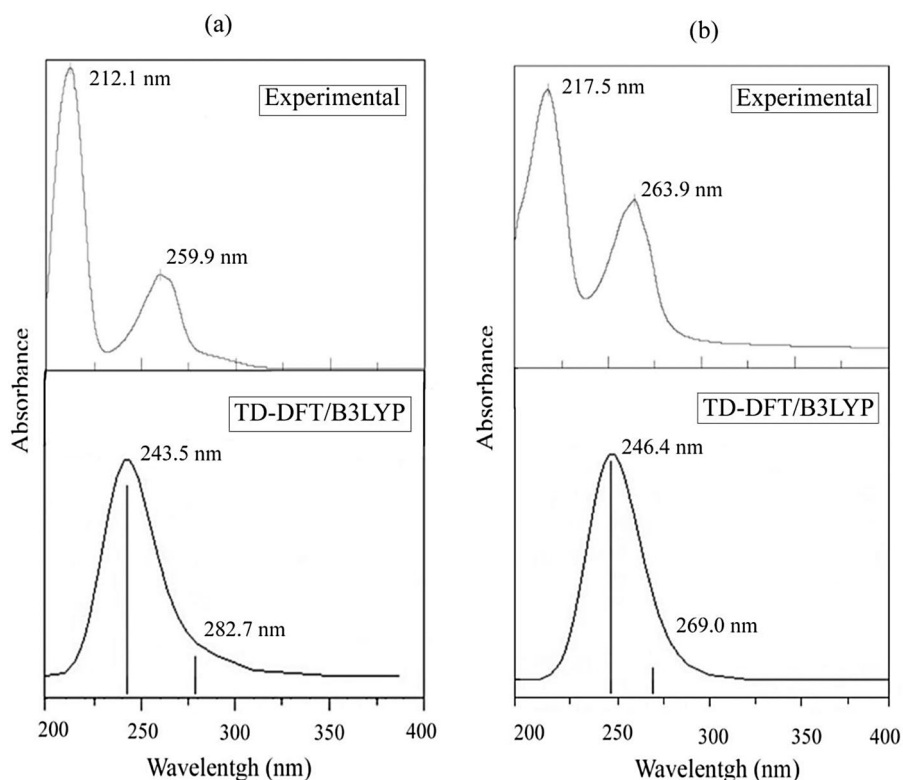


**Figure 10.** UV-Visible Spectrum of (a) CM and (b) DCM.

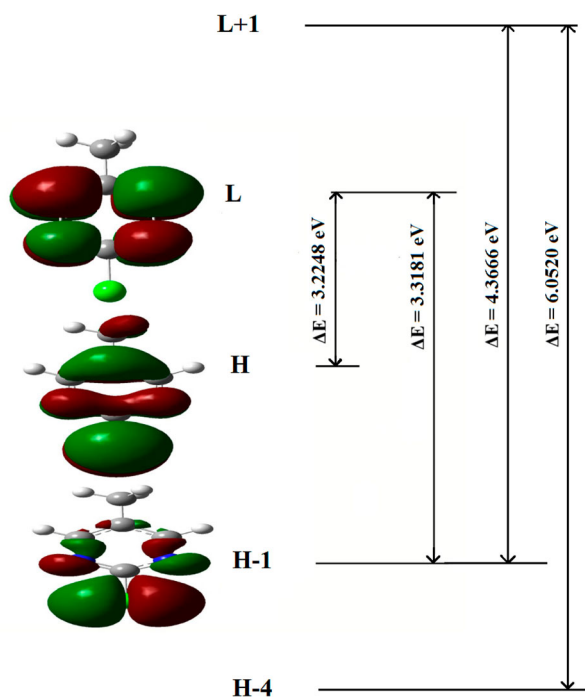


Figure 11. (Colour online) Frontier molecular orbitals of CM.

#### 4.4. Molecular electrostatic surface potential (MESP)

MESP analysis is a useful technique to understand the charge distribution in a given molecule (including biomolecules and drugs) in three dimensions and is often used to determine chemical reactivities, hydrogen bond interactions, electrophilic and nucleophilic regions [60,61]. It plays a key role in studying the relationship between physicochemical properties and molecular structure. It also presents a visual approach for knowing the relative polarity of a molecule. The positive electrostatic potential corresponds to the repulsion of the proton by the atomic nucleus in regions of low electron density, while the negative electrostatic potential corresponds to the attraction of the proton by high electron density regions of the molecule.

MESP can be evaluated by mapping molecular electrostatic potential (MEP)  $V(\mathbf{r})$  onto the iso-electron density surface. The MESP at any given point  $r(x, y, z)$  is the sum of two opposing interaction energies (positive and negative) and can be expressed as [62]

$$V(\mathbf{r}) = \sum_A \frac{Z_A}{|\mathbf{R}_A - \mathbf{r}|} - \int \frac{\rho(\mathbf{r}') d\mathbf{r}'}{|\mathbf{r}' - \mathbf{r}|}$$

Table 4. Frontier molecular orbital parameters of CM and DCM by DFT/B3LYP/6-311++G(d,p) method.

Frontier molecular orbital parameter	Value (in eV)	
	CM	DCM
HOMO energy	-8.4720	-8.4159
LUMO energy	-5.2472	-4.7927
Frontier molecular orbital energy gap	3.2248	3.6232
Ionisation energy (I)	8.4720	8.4159
Electron affinity (A)	5.2472	4.7927
Global hardness ( $\eta$ )	1.6124	1.8116
Global softness (S)	0.3101	0.2760
Chemical potential ( $\mu$ )	-6.8596	-6.6043
Electronegativity ( $\chi$ )	6.8596	6.6043
Global electrophilicity power ( $\omega$ )	14.5915	12.0382

where  $Z_A$  is the nuclear charge on the nucleus A;  $\mathbf{R}_A$  is the position of A with respect to an arbitrary origin;  $\mathbf{r}$  is the position of any point, where  $V(\mathbf{r})$  is required in the space surrounding the molecule, with respect to the arbitrary origin;  $\mathbf{r}'$  is the position of the electron in the molecule, with respect to the arbitrary origin;  $\rho(\mathbf{r}')$  is electronic density function at the point  $\mathbf{r}'$ .

The first and second terms represent the contributions to the potential due to nuclei and electrons, respectively. The positive interaction energy arises from the interaction of nuclei of the molecule with a positive test charge located at  $\mathbf{r}$ , whereas the negative interaction energy originates from the interaction of electrons of the molecule with the same test charge at  $\mathbf{r}$  [63]. The total electron density and MESP surfaces of the molecules CM and DCM are evaluated by using DFT/B3LYP/6-311++G(d,p) level of theory. It is customary to use a colour scheme in MESP diagrams. In this scheme, the negative electrostatic potentials are represented in red, the intensity of which is proportional to the absolute value of the potential energy, whereas positive electrostatic potentials are indicated in blue, while green is used for the neutral region on the surface areas.

A visual representation of molecular electrostatic potential surface that demonstrates the chemically active sites and comparative reactivity of atoms in CM and DCM is shown in Figure 12. As can be seen from the MESP map of these molecules, the red regions having the negative potential are over the electronegative nitrogen atoms of the pyrimidine ring, while the blue regions having the positive potential are over the hydrogen atoms of the pyrimidine ring and that of the methyl group (Figure 13).

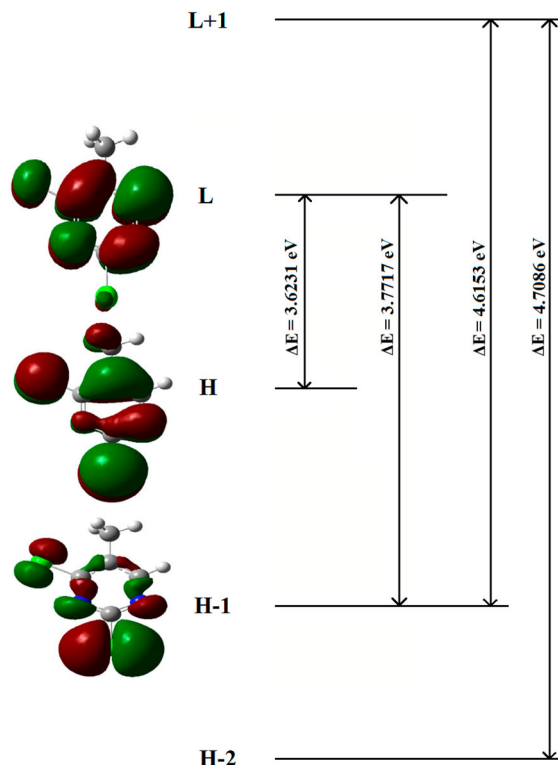
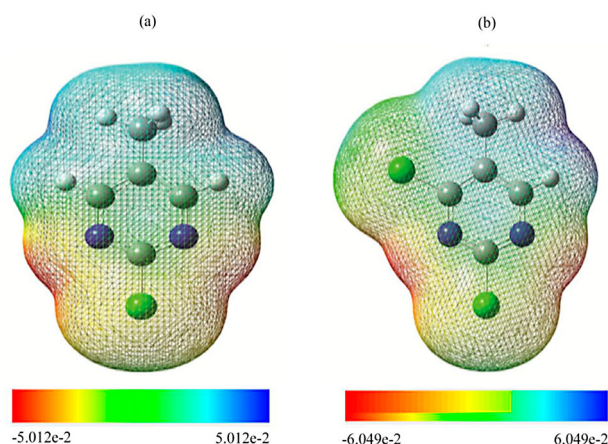


Figure 12. (Colour online) Frontier molecular orbitals of DCM.



**Figure 13.** (Colour online) Total electron density mapped with electrostatic potential surface of (a) CM and (b) DCM.

**Table 5.** Thermodynamic parameters (for one mole of perfect gas at one atm.) and rotational constants of CM and DCM.

Thermodynamic parameters	Value CM	DCM
SCF Energy (Hartree)	-763.347	-1222.972
Total energy (thermal), $E_{\text{total}}$ (kcal mol <sup>-1</sup> )	63.555	58.272
Heat capacity at const. volume, $C_V$ (cal mol <sup>-1</sup> K <sup>-1</sup> )	25.163	28.840
Heat capacity at const. pressure, $C_P$ (cal mol <sup>-1</sup> K <sup>-1</sup> )	27.149	30.826
Entropy, $S$ (cal mol <sup>-1</sup> K <sup>-1</sup> )	87.336	90.157
Vibrational energy, $E_{\text{vib}}$ (kcal mol <sup>-1</sup> )	61.778	56.494
Zero-point vibrational energy, $E_0$ (kcal mol <sup>-1</sup> )	59.052	53.214
Rotational constants (GHz)		
A	5.937	2.163
B	1.020	0.781
C	0.875	0.576

#### 4.5. Thermodynamic parameters and rotational constants

The standard thermodynamic functions such as SCF energy, specific heat capacity at constant volume ( $C_V$ ), entropy ( $S$ ),

vibrational energy ( $E_{\text{vib}}$ ), zero-point energy ( $E_0$ ) and rotational constants ( $A$ ,  $B$  and  $C$ ) are determined using rigid rotor harmonic oscillator approximation [64–66] using DFT/B3LYP/6-311++G(d,p) level of theory and are depicted in Table 5.

In this study, the rotational constants  $A$ ,  $B$  and  $C$  are calculated at 5.937, 1.020 and 0.875 GHz for CM; and 2.163, 0.781 and 0.576 GHz for DCM, respectively. All these thermodynamic calculations were done in gas phase and pertained to one mole of perfect gas at one atm. As per the second law of thermodynamics in thermo chemical field [67], the parameters presented in Table 5 can be used to compute other thermodynamic energies and help to estimate the directions of chemical reactions.

#### 4.6. Natural bond orbitals (NBO) analyses

The results of NBO analysis for CM and DCM are reported in Tables 6 and 7, respectively. Only major contributors to the stabilisation energy are included in these tables. In NBO method, the orbitals are selected theoretically such that the highest possible percentage of the electron density (ED) is included. Hence, it provides a convenient means for elucidation of a clear ‘natural Lewis structure’ of the wave function ( $\Psi$ ). Further, it also demonstrates the conjugative interaction due to charge transfer at a molecular level and reveals the existence of intra- and inter-molecular bonding and interaction among bonds precisely. The significant value of stabilisation Energy  $E(2)$  implies strong interaction between the electron donors and electron acceptors, resulting in a greater extent of conjugation of the entire structure. The delocalisation of electron density, between occupied Lewis-type (bonding or lone pair) NBO orbitals and empty non-Lewis (anti bonding or Rydberg) NBO orbitals indicates stabilisation of donor–acceptor interaction. The overlapping between bonding  $\pi$ -orbitals and anti-bonding  $\pi^*$ -orbitals results in intra-molecular hyper conjugative interactions. This leads to intra-

**Table 6.** Second-order perturbation energies  $E(2)$  (kJ/mol) corresponding to the most important charge transfer interaction (donor–acceptor) in CM by DFT/B3LYP/6-311++G(d,p) method (only major contributors to stabilisation energy are given).

NBO(i)	Type	ED/e	NBO(j)	Type	ED/e	$E(2)^a$ (kJ/mol)	$E_{(j)}-E_{(i)}^b$ (a.u.)	$F_{(i,j)}^c$ (a.u.)
N1-C6	$\sigma$	1.9765	C2-Cl7	$\sigma^*$	0.0700	5.13	0.98	0.064
	$\pi$	1.7100	C2-N3	$\pi^*$	0.4149	34.67	0.30	0.093
			C4-C5	$\pi^*$	0.2936	12.03	0.33	0.056
C2-N3	$\pi$	1.7142	N1-C6	$\pi^*$	0.3543	11.26	0.32	0.054
			C4-C5	$\pi^*$	0.2936	25.50	0.34	0.084
N3-C4	$\sigma$	1.9763	C2-Cl7	$\sigma^*$	0.0700	5.21	0.98	0.065
	$\pi$	1.6080	N1-C6	$\pi^*$	0.3543	31.63	0.26	0.082
C4-C5	$\pi$	1.6080	C2-N3	$\pi^*$	0.4149	16.92	0.25	0.059
			C2-N3	$\sigma^*$	0.0448	4.10	1.06	0.059
C4-H8	$\sigma$	1.9826	N1-C2	$\sigma^*$	0.0453	4.15	1.06	0.060
C6-H9	$\sigma$	1.9824	C5-C6	$\sigma^*$	0.0323	4.69	1.06	0.063
C10-H11	$\sigma$	1.9886	C2-N3	$\sigma^*$	0.0448	12.37	0.88	0.094
LP N1	$\sigma$	1.9056	C5-C6	$\sigma^*$	0.0323	8.34	0.91	0.079
LP N3	$\sigma$	1.9044	N1-C2	$\sigma^*$	0.0453	12.48	0.88	0.095
			C2-Cl7	$\sigma^*$	0.0700	4.00	0.50	0.040
LP Cl7	$\pi$	1.9670	C4-C5	$\sigma^*$	0.0315	8.31	0.91	0.079
			N1-C2	$\sigma^*$	0.0453	5.55	0.82	0.060
			C2-N3	$\sigma^*$	0.0448	5.55	0.83	0.061
	$\pi$	1.9063	C2-N3	$\pi^*$	0.4149	16.70	0.29	0.067

<sup>a</sup> $E(2)$  means energy of hyper conjugative interaction (stabilisation energy).

<sup>b</sup>Energy difference between donor (i) and acceptor (j) natural bond orbitals.

<sup>c</sup> $F_{(i,j)}$  is the Fock matrix element between i and j natural bond orbitals.

a.u.: atomic unit.

**Table 7.** Second-order perturbation energies  $E(2)$  (kJ/mol) corresponding to the most important charge transfer interaction (donor–acceptor) in DCM by DFT/B3LYP/6-311++G(d,p) method (only major contributors to stabilisation energy are given).

NBO(i)	Type	ED/e	NBO(j)	Type	ED/e	$E(2)^a$ (kJ/mol)	$E(j)-E(i)^b$ (a.u)	$F(i,j)^c$ (a.u)
N1-C2	$\pi$	1.7332	N3-C4	$\pi^*$	0.4387	10.82	0.31	0.054
			C5-C6	$\pi^*$	0.2696	24.86	0.35	0.084
N1-C6	$\sigma$	1.9758	C2-C17	$\sigma^*$	0.0671	5.47	0.98	0.066
C2-N3	$\sigma$	1.9802	C4-C18	$\sigma^*$	0.0603	4.98	1.01	0.064
N3-C4	$\sigma$	1.9799	C2-C17	$\sigma^*$	0.0671	4.31	1.02	0.060
	$\pi$	1.7367	N1-C2	$\pi^*$	0.4205	31.11	0.31	0.092
			C5-C6	$\pi^*$	0.2696	10.34	0.36	0.054
C5-C6	$\sigma$	1.9719	C4-C18	$\sigma^*$	0.0603	5.81	0.86	0.063
	$\pi$	1.5932	N1-C2	$\pi^*$	0.4205	17.48	0.24	0.058
			N3-C4	$\pi^*$	0.4387	35.16	0.24	0.083
C10-H11	$\sigma$	1.9876	C4-C5	$\sigma^*$	0.0443	4.91	1.03	0.064
LP N1	$\sigma$	1.9067	C2-N3	$\sigma^*$	0.0476	12.74	0.87	0.095
			C5-C6	$\sigma^*$	0.0321	8.40	0.92	0.080
LP N3	$\sigma$	1.8898	N1-C2	$\sigma^*$	0.0436	12.10	0.89	0.094
			C2-C17	$\sigma^*$	0.0671	4.26	0.50	0.042
			C4-C5	$\sigma^*$	0.0443	9.62	0.90	0.085
			C4-C18	$\sigma^*$	0.0603	4.82	0.50	0.044
LP C17	$\pi$	1.9668	N1-C2	$\sigma^*$	0.0436	5.55	0.84	0.061
			C2-N3	$\sigma^*$	0.0476	5.80	0.82	0.062
			N1-C2	$\pi^*$	0.4205	16.64	0.29	0.068
LP C18	$\pi$	1.9658	N3-C4	$\sigma^*$	0.0305	6.17	0.84	0.064
	$\pi$	1.9013	N3-C4	$\pi^*$	0.4387	16.87	0.29	0.069

Note: a.u., atomic unit.

<sup>a</sup> $E(2)$  means energy of hyper conjugative interaction (stabilisation energy).

<sup>b</sup>Energy difference between donor (i) and acceptor (j) natural bond orbitals.

<sup>c</sup> $F(i,j)$  is the Fock matrix element between i and j natural bond orbitals.

molecular charge transfer (ICT) that stabilises the system. Such interactions are observed as an enhancement in the electron density in pyrimidine C2-N3, C4-C5 and N1-C6 anti-bonding orbitals. They weaken the corresponding bonds. The electron density for CM at the conjugated  $\pi$ -bonds of the pyrimidine ring is between 1.6080 and 1.7142 (see Table 6), whereas the corresponding values for  $\pi^*$ -anti-bonds is in the range 0.2936–0.4149. As a consequence of this intense charge delocalisation, the molecule generates total stabilisation energy 148.71 kcal mol<sup>-1</sup> from the pyrimidine ring alone. The interactions  $\pi(N1-C6) \rightarrow \pi^*(C2-N3, C4-C5)$ ;  $\pi(C2-N3) \rightarrow \pi^*(N1-C6, C4-C5)$ ;  $\pi(C4-C5) \rightarrow \pi^*(N1-C6, C2-N3)$ ; LP C17  $\rightarrow \pi^*(C2-N3)$  possess stabilisation energy in the range 11.26–34.67 kcal mol<sup>-1</sup>, respectively. As a result of  $\pi$ -electron cloud movement from donor to acceptor, the molecule gets more polarised. Similar conclusions can be made for DCM by examining the data reported in Table 7.

## 5. Conclusions

The following inferences can be made on the basis of the investigation carried out.

- (1) Both 2-chloro-5-methylpyrimidine and 2,4-dichloro-5-methylpyrimidine molecules exhibit  $C_1$  point group symmetry in the ground state. The dihedral angles are 0° and 180°, respectively, for CM and DCM, in the ground state (this is an around inter-link C–C bond connecting pyrimidine ring and methyl moiety).
- (2) Theoretical geometry parameters show good agreement for 2-chloro-5-methylpyrimidine and 2,4-dichloro-5-methylpyrimidine with their experimental counterparts in related molecules. Further, the existence of inter-molecular hydrogen bond is predicted in their dimers.

- (3) Experimental and computed vibrational frequencies agree well for both molecules.
- (4) All fundamentals of both CM and DCM are assigned unambiguously for the first time.
- (5) Small value of HOMO–LUMO energy gap signifies that the molecules are easily polarisable. Similarly, negative value of chemical potential indicates that the molecules are stable.
- (6) The MESP map of both molecules shows that the negative potentials are over the electronegative nitrogen atoms of the pyrimidine ring, whereas the positive potentials are over the hydrogen atoms of the pyrimidine ring and that of the methyl group.

## Acknowledgements

The authors sincerely acknowledge Sophisticated Analytical Instrumentation Facility (SAIF), IIT Madras, Chennai, India, for spectral measurements (IR & Raman). They are also grateful to NIPER, Hyderabad, for recording UV-Visible spectra.

## Disclosure statement

No potential conflict of interest was reported by the author(s).

## ORCID

B. Venkatram Reddy  <http://orcid.org/0000-0001-6516-7731>

## References

- [1] Srishailam K, Venkatram Reddy B, Ramana Rao G. Investigation of torsional potentials, hindered rotation, molecular structure and vibrational properties of some biphenyl carboxaldehydes using

- spectroscopic techniques and density functional formalism. *J Mol Struct.* **2019**;1196:139–161.
- [2] Ravindranath L, Venkatram Reddy B. Theoretical and experimental study of torsional potentials, molecular structure (monomer and dimer), vibrational analysis and molecular characteristics of some dimethyl bipyridines. *J Mol Struct.* **2020**;1200:127089.
- [3] Venkata Ramana Rao P, Srishailam K, Venkatram Reddy B, et al. Theoretical (DFT) and experimental (FT-IR & FT Raman) approach to investigate the molecular geometry and vibrational properties of 2, 5-and 2, 6-dihydroxytoluenes. *J Mol Struct.* **2021**;1240:130617.
- [4] Brown DJ. Pyrimidines and their benzo derivatives, in comprehensive heterocyclic chemistry. In: AR Katritzky, CW Rees, Oxford: Pergamon Press; **1984**.
- [5] Inoue M, Hashimoto K. Jpn. Kokai Tokyo Koho, Jp. (Japanese Patent No.) 03204877 [91,204,877]. *Chem Abstr.* **1992**;116:6580z.
- [6] Goto K. Jpn. Kokai Tokyo Koho, Jp. (Japanese Patent No.) 03215488 [91,215,488]. *Chem Abstr.* **1992**;116:128962w.
- [7] Goto K, Hashimoto K, Kanai K. Jpn. Kokai Tokyo Koho, Jp.(Japanese Patent No.) 63,168,685 [88,198,685]. *Chem Abstr.* **1989**;110:23911b.
- [8] Santagati A, Modica M, Santagati M, et al. *Chem Abstr.* **1994**;49:64, .1994;120:323518r.
- [9] Vou Borstel RW, Bamat MK, Hiltran BM. PCT int. Appl. WO. 690.11.15. *Chem Abstr.* **1996**;124:250921n.
- [10] Da Settimo A, Da Settimo F, Marini AM, et al. Synthesis, DNA binding and in vitro antiproliferative activity of purinoquinazoline, pyridopyrimidopurine and pyridopyrimidobenzimidazole derivatives as potential antitumor agents. *Eur J Med Chem.* **1998**;33:685–696.
- [11] Russo F, Romo G, Santagati NA, et al. Synthesis of new thienopyrimidobenzothiazoles and thienopyrimidobenzoxazoles with analgesic and antiinflammatory properties. *Eur J Med Chem.* **1994**;29:569–578.
- [12] Sondhi SM, Singhal N, Verma RP, et al. Synthesis and antiinflammatory and anticancer activity evaluation of some condensed pyrimidines. *Monatshefte für Chemie.* **2000**;131:501–509.
- [13] Sondhi SM, Johar M, Singhal N, et al. Synthesis and anticancer, antiinflammatory, and analgesic activity evaluation of some sulfa drug and acridine derivatives. *Monatshefte für Chemie.* **2000**;131:511–520.
- [14] Sondhi SM, Singhal N, Verma RP, et al. Synthesis of hemin and porphyrin derivatives and their evaluation for anticancer activity. *Indian J Chem Sec B.* **2001**;40B:113–119.
- [15] Tang G, Kertesz DJ, Yang M, et al. Exploration of piperidine-4-yl-aminopyrimidines as HIV-1 reverse transcriptase inhibitors. *N-phenyl derivatives with broad potency against resistant mutant viruses.* *Bioorg Med Chem Lett.* **2010**;20:6020–6023.
- [16] Gazivoda Kraljevic T, Krištafor S, Šuman L, et al. Synthesis, X-ray crystal structure study and antitumoral evaluations of 5,6-disubstituted pyrimidine derivatives. *Bioorg Med Chem.* **2010**;18:2704–2712.
- [17] Szterner P, Amaral LMPF, Morais VMF, et al. Thermochemical study of dichloromethyl pyrimidine isomers. *J Chem Thermodynamics.* **2016**;100:148–155.
- [18] Joshi BD. Structural, electronic and vibrational study of 4, 6-dichloro-5-methylpyrimidine: A DFT approach. *J Institute Sci Tech.* **2017**;22(1):51–60.
- [19] Medjani M, Hamdouni N, Brihi O, et al. Crystal structure of 4,6-dichloro-5-methylpyrimidine. *Acta Cryst.* **2015**;E71:o1073–o1074.
- [20] Furberg S, Groggaard J, Smedsrud B. Effect of substitution on pyrimidine. The crystal structures of pyrimidine and its 5-methyl, 2-chloro and 2-amino derivatives. *Acta Chemica Scandinavica B.* **1979**;33:715–724.
- [21] Dennington R, Keith T, Millam J. Gauss View, Version 5.0. Semichem Inc., Shawnee Mission; **2009**.
- [22] Frisch MJ. Gaussian 09, Revision B.01. Wallingford (CT): Gaussian, Inc.; **2010**.
- [23] Becke AD. Density-functional thermochemistry. III. The role of exact exchange. *J Chem Phys.* **1993**;98:5648–5652.
- [24] Lee C, Yang W, Parr RG. Development of the colle-salvetti correlation-energy formula into a functional of the electron density. *Phys Rev B.* **1988**;37:785–789.
- [25] Latajka Z, Person WB, Morokuma K. An ab initio calculation of the infrared spectrum and tautomerism of guanine. *J Mol Struct (Theochem).* **1986**;135:253–266.
- [26] Kerezturny G, Holly S, Besenyel G, et al. Vibrational spectra of monothiocarbamates-II. IR and Raman spectra, vibrational assignment, conformational analysis and ab initio calculations of S-methyl-N,N-dimethylthiocarbamate. *Spectrochim Acta Part A.* **1993**;49:2007–2026.
- [27] Kerezturny G. In: Chalmers JM, Griffiths PR, editors. Raman spectroscopy: theory in hand book of vibrational spectroscopy, vol.1. New York: Wiley and sons Ltd; **2002**. p. 71–87.
- [28] Rahut G, Pulay P. Transferable scaling factors for density functional derived vibrational force fields. *J Phys Chem.* **1995**;99:3093–3100.
- [29] Pulay P, Fogarasi G, Pongor G, et al. Combination of theoretical Ab initio and experimental information to obtain reliable harmonic force constants. Scaled Quantum Mechanical (SQM) force fields for glyoxal, acrolein, butadiene, formaldehyde, and ethylene. *J Am Chem Soc.* **1983**;105(24):7037–7047.
- [30] Arenas JF, Tocón IL, Otero JC, et al. Vibrational spectra of methylpyridines. *J Mol Struct.* **1999**;476:139–150.
- [31] Fogarasi G, Zhou X, Tayler PW, et al. The calculation of ab initio molecular geometries: efficient optimization by natural internal coordinates and empirical correction by offset forces. *J Am Chem Soc.* **1992**;114:8191–8201.
- [32] Sundius T. Molvib - A flexible program for force field calculations. *J Mol Struct.* **1990**;218:321–326.
- [33] Sundius T. Scaling of ab initio force fields by MOLVIB. *Vib Spectrosc.* **2002**;29:89–95.
- [34] Glendening ED, Reed AE, Carpenter JE, et al. NBO Version 3.1, TCI. Madison: University of Wisconsin; **1998**.
- [35] Paizs B, Fogarasi G, Pulay P. An efficient direct method for geometry optimization of large molecules in internal coordinates. *J Chem Phys.* **1998**;109:6571–6576.
- [36] Steiner T. C-H...O hydrogen bonding in crystals. *Crystallogr Rev.* **2003**;9:177–228.
- [37] Steiner T, Desiraju GR. Distinction between the weak hydrogen bond and the Van der Waals interaction. *Chem Commun.* **1998**: 891–892.
- [38] Desiraju GR. C-H...O and other weak hydrogen bonds. from crystal engineering to virtual screening. *Chem Commun.* **2005**: 2995–3001.
- [39] Biegler-König F, Schönbohm J. Update of the AIM2000-program for atoms in M molecules. *J Comput Chem.* **2002**;23:1489–1494.
- [40] Wilson EB, Jr. The Normal modes and frequencies of vibration of the regular plane hexagon model of the benzene molecule. *Phys Rev.* **1934**;45:706–714.
- [41] Prabavathi N, Senthil Nayaki N, Venkatram Reddy B. Molecular structure, vibrational spectra, natural bond orbital and thermodynamic analysis of 3,6-dichloro-4-methylpyridazine and 3,6-dichloropyridazine-4-carboxylic acid by dft approach. *Spectrochim Acta A.* **2015**;136:1134–1148.
- [42] Ojha JK, Venkatram Reddy B, Ramana Rao G. Vibrational analysis and valence force field for nitrotoluenes, dimethylanilines and some substituted methylbenzenes. *Spectrochim Acta A.* **2012**;96:632–643.
- [43] Parrish RM., Hohenstein EG, McMahon PL, et al. Quantum computation of electronic transitions using a variational Quantum eigensolver. *Phy Rev Lett.* **2019**;122(1-6):230401.
- [44] Jacquemin D, Perpète EA, Ciofini I, et al. Accurate simulation of optical properties in dyes Acc. Chem Res. **2009**;42:326–334.
- [45] Jacquemin D, Preat J, Wathelet V, et al. Thioindigo dyes: highly accurate visible spectra with TD-DFT. *J Am Chem Soc.* **2006**;128:2072–2083.
- [46] Ciofini I, Adamo C. Accurate evaluation of valence and low-lying Rydberg states with standard time-dependent density functional theory. *J Phys Chem A.* **2007**;111:5549–5556.
- [47] Maric D, Burrows JP. Application of a Gaussian Distribution Function to describe molecular UV-visible absorption continua .1. Theory, *J Phys Chem A.* **1996**;100:8645–8659.
- [48] Maric D, Crowley JN, Burrows JP. Application of a Gaussian Distribution Function to describe molecular UV-Visible

- absorption continua. 2. The UV spectra of  $RO_2^{\bullet}$  radicals. *J Phys Chem A*. 1997;101:2561–2567.
- [49] Bremond EAG, Kieffer J, Adamo C. A reliable method for fitting TD-DFT transitions to experimental UV–visible spectra. *J Mol Struct (Theochem)*. 2010;954:52–56.
- [50] Jacquemin D, Perpète EA. Ab initio calculations of the colour of closed-ring diarylethenes: TD-DFT estimates for molecular switches chem. *Phys Lett*. 2006;429:147–152.
- [51] Preat J, Michaux C, Lewalle A, et al. Delocalisation in conjugated triazene chromophores: insights from theory chem. *Phys Lett*. 2008;451:37–42.
- [52] Scalmani G, Frisch MJ. Continuous surface charge polarizable continuum models of solvation. I. General formalism. *J Chem Phys*. 2010;132:114110.
- [53] Fukui K. Role of frontier orbitals in chemical reactions. *Science*. 1982;218:747–754.
- [54] Koopmans TA. Ordering of wave functions and eigen energies of the individual electrons of an atom. *Physica*. 1933;1:104–113.
- [55] Choi CH, Kertez M. Conformational information from vibrational spectra of styrene, trans-stilbene, and cis-stilbene. *J Phys Chem A*. 1997;101:3823–3831.
- [56] Sinha L, Prasad O, Narayan V, et al. Raman, FT-IR spectroscopic analysis and first-order hyperpolarizability of 3-benzoyl-5-chlorouracil by first principles. *J Mol Simul*. 2011;37:153–163.
- [57] Lewis DFV, Ioannides C, Parke DV. Interaction of a series of nitriles with the alcohol-inducible isoform of P450: computer analysis of structure-activity relationships. *Xenobiotica*. 1994;24:401–408.
- [58] Kosar D, Albayrak C. Spectroscopic investigations and quantum chemical computational study of (E)-4-methoxy-2-[(p-tolylimino)-methyl]phenol. *Spectrochim Acta A*. 2011;78:160–167.
- [59] Nakano M, Fujita H, Takahata M, et al. Theoretical study on second hyperpolarizabilities of phenylacetylene dendrimer: toward an understanding of structure-property relation in NLO responses of fractal antenna dendrimers. *J Am Chem Soc*. 2002;124:9648–9655.
- [60] Luque FJ, López JM, Orozco M. Perspective on “electrostatic interactions of a solute with a continuum. A direct utilization of ab initio molecular potentials for the prevision of solvent effects”. *Theo Chem Accounts*. 2000;103:343–345.
- [61] Scrocco E, Tomasi J. *Topics in current chemistry, New concepts-II*. New York. 1973.
- [62] Kalaiarasi N, Manivarman S. Synthesis, spectroscopic characterization, computational exploration Of 6-(2-(2, 4-dinitrophenylhydrazano)-tetrahydro-2-thioxopyrimidin-4(1h)-one. *Oriental J Chem*. 2017;33(1):304–317.
- [63] Politzer P, Murray JS. The fundamental nature and role of the electrostatic potential in atoms and molecules. *Theor Chem Acc*. 2002;108:134–142.
- [64] Herzberg G. *Infrared and Raman spectra of polyatomic molecules*. New York (NY): D. Van Nostrand; 1945.
- [65] Pitzer KS, Gwinn WD. Energy levels and thermodynamic functions for molecules with internal rotation: I. Rigid frame with attached tops. *Mol Struct and Stat Thermodynamics*. 1993: 33–46.
- [66] Ghahremanpour MM, Van Maaren PJ, Ditz JC, et al. Large-scale calculations of gas phase thermochemistry: enthalpy of formation, standard entropy, and heat capacity. *J Chem Phys*. 2016;145:114305.
- [67] Balachandran V, Karunakaran V. Quantum mechanical study of the structure and vibrational spectroscopic (FT-IR and FT-Raman), first-order hyperpolarizability, NBO and HOMO–LUMO studies of 4-bromo-3-nitroanisole. *Spectrochim Acta, Part A*. 2013;106:284–298.